Progress in Physics of Applied Materials 7 (2027), Serial Number 15, 9-15

Semnan University

Progress in Physics of Applied Materials

journal homepage: https://ppam.semnan.ac.ir/

Optimization of the Magnetothermal Properties of LGSMO–MXene–Based Nanocomposite for Magnetic Refrigeration Applications

A.I. Kagramanian [a*], E.A. Kanareykin [a], Y.I. Spichkin [a,b], M.H. Ehsani [c], A.M. Tishin [a,b]

[a]*Moscow Institute of Physics and Technology (MIPT), Institutskiy per. 9, Dolgoprudny, 141701, Moscow Region, Russia*
[b]*Lomonosov Moscow State University (MSU), Faculty of Physics, Leninskie Gory, 1, Moscow, 119991, Russia*
[c]*Faculty of Physics, Semnan University, Semnan 35195-363, Iran*

ARTICLE INFO

Article history:
Received: 30 June 2026
Revised: 25 July 2026
Accepted: 28 July 2026
Published online: 7 September 2026

Keywords:
magnetocaloric effect;
magnetic refrigeration;
LGSMO;
MXene;
ellipsoidal inclusion;
aspect ratio optimization;
demagnetization factor;
finite element method;
Gaussian process regression;
fractal packing.

ABSTRACT

The optimization of magnetocaloric heat transfer efficiency in a $La_{0.5}Gd_{0.1}Sr_{0.4}MnO_3$ (LGSMO)/$Ti_3C_2T_x$ MXene composite for solid-state magnetic refrigeration was performed. The effect of the orientation angle α of ellipsoidal LGSMO inclusions relative to the anisotropic MXene matrix and the inclusion aspect ratio λ on the heat removal rate, characterized by the target function $J = \Delta T_{ad}/\tau$, where ΔT_{ad} is the adiabatic temperature rise and τ is the thermal relaxation time, was investigated using the finite element method. For a single grain, the optimal orientation was found at α = 90°, with the major axis aligned in the high-conductivity plane of MXene, and β = 0°, where β is the angle between the major axis and the external magnetic field direction, minimizing the demagnetization factor and maximizing the internal field H_{int}. The analysis was further extended to a fractal hexagonal packing of ellipsoidal grains by introducing an effective target function $J_{eff} = J \cdot \eta$, which accounts for the volume fraction η of LGSMO in the composite. The optimal aspect ratio for the packed system was found at $\lambda \approx 5$, balancing the competing effects of improved single-grain heat transfer and reduced packing density at higher λ. The model was further augmented by introducing cylindrical isothermal channels aligned along the high-conductivity direction of the MXene matrix as distributed heat sinks, which shifted the optimal aspect ratio to $\lambda^* \approx 2.3$, reflecting the dominant role of grain-to-channel thermal resistance in determining the heat removal efficiency of the active composite.

1. Introduction

Magnetic refrigeration based on the magnetocaloric effect (MCE) is widely regarded as a promising alternative to conventional vapor-compression cooling due to its higher thermodynamic efficiency and reduced environmental impact [1, 2]. The MCE manifests as an adiabatic temperature change ΔT_{ad} upon application or removal of an external magnetic field and is particularly pronounced near the Curie temperature T_C of ferromagnetic materials. Among magnetocaloric materials, lanthanum–strontium manganites $La_{1-x}Sr_xMnO_3$ (LSMO) have attracted significant attention because their Curie temperature can be tuned to the vicinity of room temperature while maintaining a relatively large MCE and good chemical stability [3, 4, 5]. It has also been shown that partial substitution of La with Gd enables further tuning of the magnetic transition temperature without substantial degradation of the magnetocaloric response [4, 6]. In addition, thermal transport properties of related manganite compounds have been systematically investigated [7], providing a foundation for modeling heat transfer in composite systems. The performance of a magnetocaloric device is determined not only by the

* Corresponding authors.
E-mail addresses: kagramanian@amtc.org

Cite this article as:

Kagramanian, A.I., Kanareykin, E.A., Spichkin, Y.I., Ehsani, M.H. and Tishin, A.M., 2026. Optimization of the Magnetothermal Properties of LGSMO–MXene-Based Nanocomposite for Magnetic Refrigeration Applications. *Progress in Physics of Applied Materials*, *7*(2), pp.9-15.DOI: **10.22075/ppam.2026.41822.1245**

intrinsic properties of the active material, but also by the efficiency of heat exchange with the surroundings. In this context, $Ti_3C_2T_x$ MXene, a two-dimensional material with strongly anisotropic thermal conductivity ($k_\parallel \approx 57$ W/m·K in-plane and $k_\perp \approx 2$ W/m·K out-of-plane), represents a promising matrix for magnetocaloric composites, as it enables directional heat removal from embedded inclusions. We noted that the geometry and orientation of magnetocaloric inclusions within an anisotropic matrix had a significant impact on both magnetic and thermal characteristics of the system. In particular, the demagnetization factor affected the internal magnetic field and, consequently, the achievable ΔT_{ad}, while the characteristic thermal relaxation time τ governed the rate of heat dissipation. To analyze these coupled effects, we employed a finite-element method (FEM) to solve the magnetostatic and heat-transfer problem over a broad parameter space.

In this work, we present a numerical optimization of ellipsoidal LGSMO inclusions embedded in a $Ti_3C_2T_x$ MXene matrix. The optimization is performed with respect to three geometric parameters: the aspect ratio λ of the inclusions, the angle α between the inclusion major axis and the direction of low thermal conductivity (out-of-plane direction) of the matrix, and the angle β between the inclusion major axis and the external magnetic field. We further extend the analysis to a hierarchical hexagonal packing geometry and introduce an effective heat-removal metric that accounts for the volume fraction of the magnetocaloric phase. $Ti_3C_2T_x$ MXene represents a promising matrix for magnetocaloric composites. Advanced processing techniques, such as plasma surface treatment [8], can be utilized to modify such 2D structures for enhanced performance.

2. Model and Methods

2.1. Material Parameters

The magnetocaloric working material is $La_{0.5}Gd_{0.1}Sr_{0.4}MnO_3$ (LGSMO), a perovskite manganite with Curie temperature $T_C \approx 336$ K and adiabatic temperature rise $\Delta T_{ad}^{max} \approx 1.5$ K at an applied magnetic field of $\mu_0 H = 2$ T [4]. The density ρ = 6300 kg/m³ is typical for perovskite manganites of the La–Sr–MnO_3 family. The specific heat capacity c_p = 500 J/(kg·K) and thermal conductivity k_{LGSMO} = 2 W/(m·K) are adopted as representative values for $La_{1-x}Sr_xMnO_3$ manganites near room temperature [7]. The matrix material is $Ti_3C_2T_x$ MXene, a two-dimensional transition metal carbide with strongly anisotropic thermal conductivity. The in-plane thermal conductivity of $Ti_3C_2T_x$ MXene is strongly dependent on the film preparation method. For dense multilayered $Ti_3C_2T_x$ films, values up to 55.8 W/(m·K) have been reported [8], which we adopt as the in-plane conductivity $k_\parallel$ = 57 W/(m·K) representative of a well-consolidated MXene matrix. The out-of-plane conductivity is taken as $k_\perp$ = 2 W/(m·K), consistent with measurements on MXene thin films [9]. In the finite element model the MXene matrix is described by the diagonal thermal conductivity tensor

$$\hat{k} = \mathrm{diag}(k_\parallel,\ k_\parallel,\ k_\perp), \tag{1}$$

where the z-axis is taken perpendicular to the MXene planes.

2.2. Inclusion Geometry and Orientatio

LGSMO inclusions are modelled as prolate spheroids with volume equal to that of a reference sphere of radius R_0. The semi-axes are parametrized by the aspect ratio λ as

$$a = R_0\lambda^{\frac{2}{3}},\ b = \frac{R_0}{\lambda^{\frac{1}{3}}}, \tag{2}$$

so that the inclusion volume $V = \frac{4}{3}\pi R_0^3$ is preserved for all $\lambda \geq 1$. The spherical case corresponds to $\lambda = 1$.

The orientation of the inclusion within the MXene matrix is described by two angles (Figure 1). The angle α is defined between the major axis of the spheroid and the z-axis (the low-conductivity direction of MXene), so that α = 90° corresponds to the major axis lying in the high-conductivity plane. The angle β is defined between the major axis and the direction of the external magnetic field B_{ext}. In this figure, the in-plane directions (x, y) correspond to the high-conductivity plane of MXene ($k_\parallel$). The case shown corresponds to $B_{ext} \parallel y$.

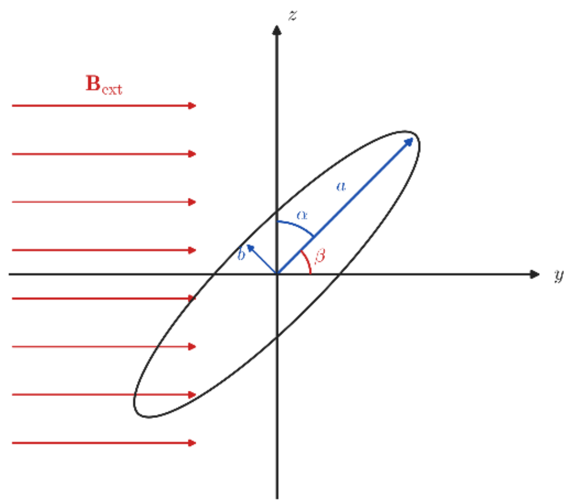

Fig. 1. Scheme of the inclusion orientation geometry.

2.3. Demagnetization Factor and Internal Field

For a prolate spheroid with eccentricity $e = \sqrt{1 - \lambda^{-2}}$, the demagnetization factors along the major and minor axes are given by the Osborn formalism [10]:

$$N_c = \frac{1 - e^2}{e^3}\left(\frac{1}{2}\frac{\ln(1+e)}{1-e} - e\right),\ N_a = \frac{1 - N_c}{2}, \tag{3}$$

where $N_c + 2N_a = 1$ by construction. For a sphere ($\lambda = 1$) one recovers $N_c = N_a = 1/3$. The effective demagnetization factor for an arbitrary angle β between the major axis and the applied field reads [1]:

$$N_{eff}(\lambda,\beta) = N_c \cos^2\beta + N_a \sin^2\beta\,. \tag{4}$$

Since N_c < N_a for any λ > 1, the effective demagnetization factor is minimized at β = 0°, which maximizes the internal magnetic field [1]:

$$H_{int} = H_{ext} - N_{eff}M_s, \tag{5}$$

where M_s = 1.5×10^5 A/m is the saturation magnetization of LGSMO [3] and $H_{ext} = B_{ext}/\mu_0$ with B_{ext} = 2 T. The adiabatic temperature rise is approximated as [1]:

$$\Delta T_{ad}(\lambda,\beta) = \Delta T_{ad}^{max}\frac{H_{int}(\lambda,\beta)}{H_{ext}} \tag{6}$$

2.4. Target Function

The efficiency of magnetocaloric heat removal from a single inclusion is characterized by the target function

$$J(\alpha,\beta,\lambda) = \frac{\Delta T_{ad}(\beta,\lambda)}{\tau(\alpha,\lambda)}, \tag{7}$$

where τ is the characteristic thermal relaxation time of the inclusion, defined as the integral of the normalized temperature response [11]:

$$\tau = \int_0^\infty \frac{\bar{T}(t) - T_f}{\bar{T}(0^+) - T_f}. \tag{8}$$

Here, $\bar{T}(t)$ is the volume-averaged temperature of the inclusion and T_f = 290 K is the fixed reservoir temperature. Since τ depends only on α and λ through the heat transfer geometry, and ΔT_{ad} depends only on β and λ through the demagnetization factor, the optimal value of β can be determined analytically: $\beta^* = 0°$ maximizes ΔT_{ad} independently of α and λ. The remaining optimization is therefore performed over the two-dimensional parameter space (α, λ) with β = 0° fixed.

2.5. Finite Element Model

The heat transfer problem is solved using FEM. The computational domain consists of a cubic MXene block of side L = 1000 μm with a single LGSMO spheroidal inclusion at the center. A fixed temperature boundary condition $T = T_f$ is imposed on all outer faces of the block, modeling an ideal thermal reservoir. The initial temperature of the entire domain is T_f.

At t = 0 the magnetocaloric effect is triggered by activating a volumetric heat source within the inclusion:

$$\dot{q} = \frac{\rho_{LGSMO}c_p\Delta T_{ad}}{t_{pulse}},\ 0 < t \le t_{pulse}, \tag{9}$$

with pulse duration t_{pulse} = 0.02 s corresponding to a field cycling frequency of 25 Hz. The volume-averaged temperature of the inclusion is monitored via a domain probe. Simulations are performed over 100 ms with a time step of 1 ms. A parametric sweep is performed over (α, λ) with $\alpha \in$ [0°,90°] and $\lambda \in$ [1, 20]. For each configuration the relaxation time τ is extracted by numerical integration of Eq. (8) applied to the probe output, and the target function J is computed using Eq. (7) with ΔT_{ad} evaluated analytically via Eqs. (4)–(6). The example of the considered configuration is shown in Figure 2. In practice, the boundary conditions of a real device would differ from this idealized reservoir. This may increase the extracted relaxation time τ.

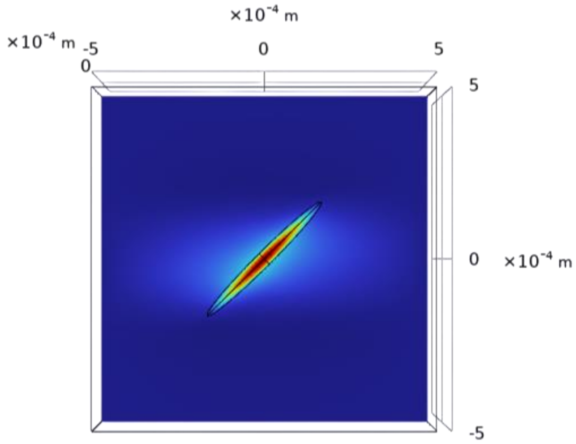

Fig. 2. Temperature distribution in the $Ti_3C_2T_x$ MXene matrix around a single LGSMO ellipsoidal inclusion for λ = 11, α = 45°, β = 0°. The y-axis points right and the z-axis points up. The color scale ranges from the reservoir temperature T_f (blue) to the peak temperature (red).

2.6. Surrogate Model and Global Optimization

To enable efficient interpolation and global optimization over the discrete parameter grid, a Gaussian Process (GP) surrogate model with a Matern covariance kernel (ν = 5/2) is trained on the finite element results using the scikit-learn library. The GP models the target function $J_{eff}(\lambda)$ as a realization of a Gaussian process, providing both a mean prediction $\mu(\lambda)$ and a posterior standard deviation $\sigma(\lambda)$:

$$\mu(\lambda) = \mathbf{k}(\lambda, \boldsymbol{X})(\mathbf{K} + \sigma_n^2\,\mathbf{I})^{-1}\mathbf{y}, \tag{10}$$

$$\sigma^2(\lambda) = k(\lambda,\lambda) - \mathbf{k}(\lambda,\boldsymbol{X})(\mathbf{K} + \sigma_n^2\mathbf{I})^{-1}\mathbf{k}(\mathbf{X},\lambda), \tag{11}$$

where $\mathbf{X}$ is the vector of training points (FEM parameter values), $\mathbf{y}$ is the corresponding vector of J_{eff} values, $\mathbf{K}$ is the covariance matrix evaluated on the training set, and σ_n^2 is the noise variance. The quantity $\sigma(\lambda)$ quantifies the interpolation uncertainty between the discrete FEM data points: it vanishes at the training points and grows in regions where data are sparse. The input feature λ is standardized prior to training. The kernel hyperparameters are optimized by maximizing the log marginal likelihood with 10 random restarts. The surrogate mean $\mu(\lambda)$ is evaluated on a dense grid of 500 points to locate the global optimum λ^* with sub-grid resolution.

2.7. Multi-Grain Packing

To extend the single-grain analysis to a realistic composite, we consider a fractal hexagonal packing of ellipsoidal grains. The elementary cell consists of seven large grains arranged in a close-packed hexagonal configuration (one central grain surrounded by six neighbors), with six smaller grains of the same aspect ratio λ placed in the interstitial voids. The ratio of the small to large grain size is $k = \sqrt{3}/(2-\sqrt{3}) \approx 6.46$, determined by the geometry of the inscribed sphere in the triangular void of the hexagonal packing.

The elementary cell is a rectangular parallelepiped whose height h is fixed at the value corresponding to λ = 13 with three packing layers:

$$h = \left(2 + 2\sqrt{3}\right) R_0 \lambda_{ref}^{\frac{2}{3}}, \;\; \lambda_{ref} = 13, \tag{12}$$

while the width and depth scale with λ as $6b(\lambda)$ and $2b(\lambda)$, respectively, where $b(\lambda) = R_0/\lambda^{1/3}$ is the minor semi-axis. As λ decreases, the grains become more rounded and more layers fit within the fixed height h; the number of layers $n(\lambda)$ is given by

$$n(\lambda) = \left\lfloor \frac{\left(\frac{\lambda_{ref}}{\lambda}\right)^{\frac{2}{3}} \left(2 + 2\sqrt{3}\right) - 2}{\sqrt{3}} + 1 \right\rfloor. \tag{13}$$

The cell is filled to capacity with grains of fixed aspect ratio λ and orientation $\alpha = \alpha^*$, $\beta = 0°$. The layers alternate between rows of 2 and 3 grains. The total number of large grains $N(\lambda)$ and the resulting LGSMO volume fraction $\eta(\lambda) = N(\lambda) V_{grain}/V_{cell}$ are computed analytically for each λ. All grains are co-oriented with $\alpha = \alpha^*$and $\beta = 0°$. The effective heat removal metric for the packed system is

$$J_{eff} = J(\alpha^*, 0, \lambda) \cdot \eta(\lambda), \tag{14}$$

where $\eta(\lambda)$ is the volume fraction of LGSMO in the elementary cell. The geometry of the fractal hexagonal packing for two representative values of the aspect ratio is illustrated in Figure 3.

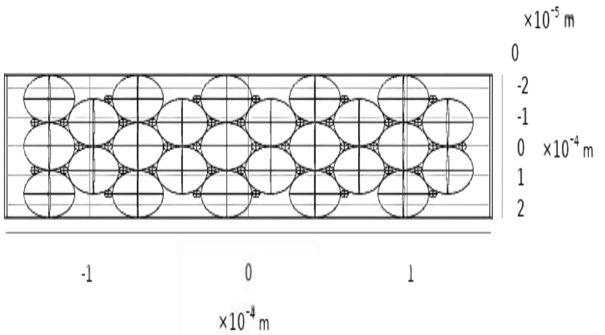

Fig. 3. Fractal hexagonal packing geometry for λ = 2.

2.8. Multi-Grain Model with Active Water Cooling

The single-grain analysis was extended to a fractal hexagonal packing of LGSMO ellipsoidal inclusions embedded in a $Ti_3C_2T_x$ MXene matrix, supplemented by cylindrical water channels aligned along the z-axis, which coincides with the direction of maximum thermal conductivity $k_{\parallel}$ = 57 W/(m·K) of the matrix. The computational domain is a rectangular parallelepiped whose lateral dimensions scale with the minor semi-axis $b(\lambda) = R_0/\lambda^{1/3}$. The domain is populated following the fractal hexagonal packing defined in Section 2.7, with all grains co-oriented at α = 90° and β = 0°.

Six cylindrical channels of radius r_{tube} are placed at the triple-point positions of the hexagonal lattice. Rather than resolving the full convective flow, each channel is modelled as a cylindrical void with a fixed-temperature boundary condition $T = T_f$ = 290 K imposed on its end faces, representing an ideal isothermal heat sink. The geometry of the assembled model is illustrated in Figure 4. Heat removal proceeds in two sequential phases: during $0 \leq t \leq t_{pulse}$ = 0.02 s (same as in Section 2.5) the magnetocaloric source $\dot{q}$ of Eq. (9) is active; thereafter the source is deactivated and heat is conducted from the LGSMO grains through the MXene matrix to the isothermal channel surfaces. A parametric sweep is performed over $\lambda \in \{1, 2, 2.5, 3, 3.5, 4, 5, 7, 9, 11, 13\}$ at fixed α = 90°, β = 0°.

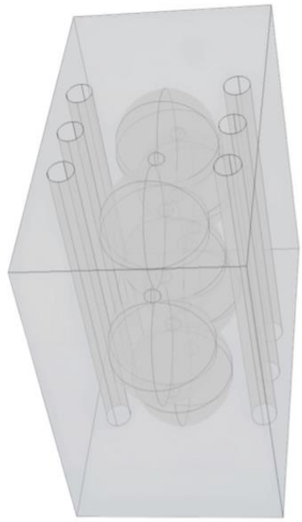

Fig. 4. Three-dimensional view of the multi-grain composite domain with active water-channel cooling. Prolate spheroidal LGSMO grains are arranged in a fractal hexagonal packing inside the $Ti_3C_2T_x$ MXene matrix; six cylindrical water channels are positioned at the triple-point vertices of the hexagonal lattice and aligned along the z-axis ($k_{\parallel}$ direction of MXene).

The relaxation time τ is extracted from each probe record by numerical integration of Eq. (8), the target function $J(\lambda)$ is computed from Eq. (7) with ΔT_{ad} evaluated analytically at β = 0°, and the effective functional is obtained as $J_{eff}(\lambda) = J(\lambda) \cdot \eta$ (Eq. (14)). A Gaussian-process surrogate is fitted to the eleven FEM data points; the posterior mean $\mu(\lambda)$ and variance $\sigma^2(\lambda)$ are evaluated by direct Cholesky factorisation of the kernel matrix according to Eqs. (10) and (11), and the surrogate is queried on a dense grid of 1000 points to identify λ^*.

3. Results

3.1. Single-Grain Optimization

The target function $J(\alpha, \lambda)$ computed from the finite element simulations at β = 0 is shown in Figure 5. The GP surrogate interpolates between the discrete FEM data points and identifies the global optimum at α^* = 88.4° and λ^* = 19.4, with J_{max} = 0.241 K ms⁻¹.

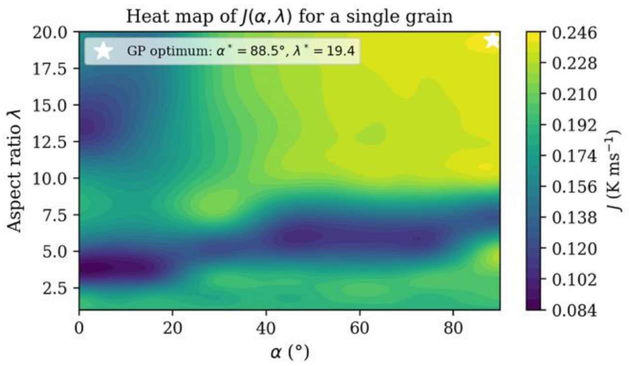

Fig. 5. Heat map of the target function $J(\alpha, \lambda)$ for a single LGSMO ellipsoidal inclusion in the $Ti_3C_2T_x$ MXene matrix at β = 0°. The color scale represents target function $J = \Delta T_{ad}/\tau$ in K ms−1, characterizing heat removal rate. The white star marks the GP optimum at α^* = 88.4°, λ^* = 19.4.

The map reveals two clear trends. First, J increases monotonically with α for all λ, with the maximum reached at α = 90°, corresponding to the major axis aligned with the high-conductivity plane of MXene. This orientation minimizes the thermal relaxation time τ by maximizing heat flux along the most conductive direction of the matrix. Second, J increases with λ and saturates at large aspect ratios: at α = 90°, the target function reaches 95% of its maximum value already at λ = 10, with only a 4.9% residual gain for λ > 10. We therefore adopt α^* = 90° and λ^* = 10 as the practical optimum, balancing heat removal efficiency against the geometric complexity of highly elongated inclusions.

3.2. Multi-Grain Packing Optimization

The effective target function $J_{eff}(\lambda) = J(\alpha^*, 0, \lambda) \cdot \eta(\lambda)$, evaluated at the optimal orientation α^* = 90°, is shown in Figure 6. The GP surrogate identifies the optimum at λ^* = 4.9, with J^*_{eff} = 0.076 K ms^{-1}.

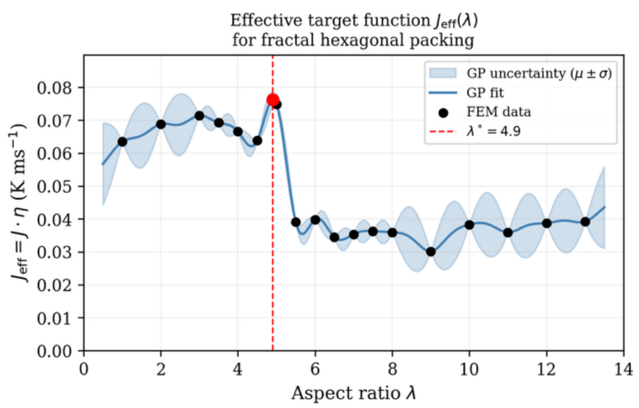

Fig. 6. Effective target function $J_{eff}(\lambda) = J{\cdot}\eta$ for the fractal hexagonal packing at α = 90°, β = 0°. Symbols show FEM data; solid line is the GP surrogate mean $\mu(\lambda)$; shaded band is the posterior uncertainty $\mu{\pm}\sigma$; dashed vertical line marks the GP optimum λ^* = 4.9.

The target function exhibits a pronounced maximum near $\lambda \approx 5$, followed by a sharp drop for λ > 5. This behaviour reflects the competition between two opposing effects. On one hand, increasing λ improves the single-grain heat removal rate J by elongating the inclusion along the high-conductivity direction of MXene. On the other hand, the fixed cell height h accommodates fewer grains as λ increases, reducing the volume fraction $\eta(\lambda)$ and thus diminishing the overall contribution of the magnetocaloric phase. The optimal aspect ratio $\lambda^* \approx 5$ represents the balance between these two competing effects.

3.3. Multi-Grain Model with Active Water Cooling

The dependence of $J_{eff}(\lambda)$ on the inclusion aspect ratio obtained from the parametric sweep is shown in Figure 7. The surrogate mean $\mu(\lambda)$ passes through all FEM data within the posterior uncertainty band $\mu \pm \sigma$, and the global optimum occurs at λ^* = 2.27, with $J^*_{eff} \approx$ 32 K s^{-1}.

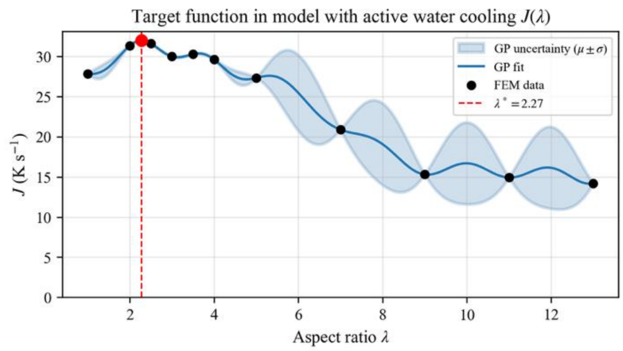

Fig. 7. Target function $J(\lambda)$ for the fractal hexagonal packing with active water-channel cooling at α = 90°, β = 0°. Symbols: FEM data; solid line: GP surrogate mean $\mu(\lambda)$; shaded band: posterior uncertainty $\mu{\pm}\sigma$; dashed line: surrogate optimum λ^*= 2.27.

The non-monotonic behavior of $J_{eff}(\lambda)$ is governed entirely by the shape dependence of the single-grain heat-removal rate $J(\lambda)$, since in the present configuration the volume fraction η of LGSMO is determined by the fixed cell geometry and is independent of λ. The optimum at λ^* = 2.27 therefore reflects a balance between two competing effects that both act through $J(\lambda) = \Delta T_{ad}(\lambda)/\tau(\lambda)$. On one hand, increasing λ reduces the demagnetization factor N_c along the major axis (Eq. (3)), which raises the internal field H_{int} and, through Eq. (6), increases ΔT_{ad}; this effect saturates for large λ as $N_c \to 0$. On the other hand, the relaxation time τ is controlled by the thermal resistance between the LGSMO grain and the nearest isothermal channel wall. For moderate elongation the grain body remains geometrically close to the surrounding channel surfaces, and heat is efficiently conducted through the MXene matrix along the high-conductivity direction $k_{\parallel}$ to the fixed-temperature sink. As λ increases beyond the optimum, the grain becomes increasingly needle-like and its tips extend far from the channels, raising the effective thermal resistance and prolonging τ despite the high in-plane conductivity of the matrix. The optimum at $\lambda^* \approx 2.3$ marks the aspect ratio at which the gain in ΔT_{ad} from reduced demagnetization can no longer compensate for the growing thermal resistance imposed by the elongated geometry of the grain relative to the fixed spatial distribution of the cooling channels.

4. Discussion

The single-grain optimization demonstrates that the thermal relaxation time τ is the dominant factor governing the heat removal rate J: aligning the major axis with the high-conductivity plane of MXene (α = 90°) provides a monotonic and substantial gain in J across all aspect ratios, while the benefit of increasing λ saturates beyond $\lambda \approx 10$. The analytical result $\beta^* = 0$ — alignment of the major axis with the external field — follows directly from the minimization of the demagnetization factor N_{eff} and is independent of the thermal geometry, confirming that the magnetic and thermal optimizations are decoupled in this system.

The multi-grain packing analysis introduces a competing effect absent at the single-grain level: the volume fraction $\eta(\lambda)$ decreases as the grains become more elongated, because the fixed cell height accommodates fewer layers. The resulting optimum at $\lambda^* \approx 5$ represents a balance between improved single-grain heat transfer and reduced packing density, and is substantially lower than the single-grain optimum $\lambda^* = 10$. The value $\lambda_{ref} = 13$ was chosen as a fixed geometric reference for the cell height h. Changing λ_{ref} would rescale $\eta(\lambda)$, but the balance between single-grain heat transfer and packing density that sets the optimum near $\lambda^* \approx 5$ is expected to remain the same.

Comparison with the fractal hexagonal packing without cooling channels, which yielded $\lambda^* = 4.9$, reveals that the introduction of active water-channel cooling shifts the optimum towards lower aspect ratios ($\lambda^* \approx 2.3$). This shift reflects the fundamentally different heat-removal mechanism: in the first case the limiting resistance is the in-matrix conduction path to the outer boundary, and elongation of the grains provides sustained gains up to $\lambda \approx 5$; in the second case the coolant channels constitute a distributed heat sink throughout the interior of the cell, so the conductive path from grain to channel is already short for moderate λ, and further elongation yields diminishing returns while the packing-density penalty $\eta(\lambda)$ continues to act. The optimum at $\lambda^* \approx 2.3$ is substantially more accessible from a fabrication perspective than the elongated morphologies required in the passive configuration.

5. Conclusion

In this work, the heat removal efficiency of an LGSMO–MXene magnetocaloric composite was optimized by tailoring the geometry and orientation of ellipsoidal inclusions. Using finite element simulations over a broad parameter space, combined with Gaussian process surrogate modelling, we identified the inclusion configurations that maximize the target function $J = \Delta T_{ad}/\tau$.

For a single inclusion, the optimal configuration ($\alpha^* = 90°$, $\beta^* = 0°$, $\lambda^* = 10$) aligns the major axis with the high-conductivity plane of MXene and with the external field, simultaneously maximizing the effective thermal conductance of the composite and the internal magnetic field. Extending the analysis to a fractal hexagonal packing, the effective heat removal rate J_{eff} was further optimized with respect to the inclusion aspect ratio, yielding $\lambda^* \approx 5$ in the passive configuration and $\lambda^* \approx 2.3$ with active water-channel cooling. In both cases, the optimized composite geometry provides a substantially enhanced heat removal rate compared to a reference spherical-inclusion ($\lambda = 1$) composite.

Funding Statement

This research was supported by the Russian Science Foundation (project no. 25-43-20052, https://rscf.ru/project/25-43-20052/).

Prof. M.H. Ehsani acknowledges the Iran National Science Foundation (INSF) (project no. 40508317, https://en.insf.org/) for supporting research.

Conflicts of Interest

The authors declare that they have no known competing financial interests or personal relationships that could have appeared to influence the work reported in this paper. M.H. Ehsani, one of the authors of this paper is the current Director-in-Charge of Progress in Physics of Applied Materials (PPAM), but he has no involvement in the peer review process used to assess this work submitted to the Journal. This paper was assessed, and the corresponding peer review managed by Dr. Sanaz Alamdari, the Executive Manager of PPAM.

Authors Contribution Statement

A.M. Tishin and M.H. Ehsani: conceptualization, validation, writing — review and editing. Yu.I. Spichkin: conceptualization, problem formulation, and supervision of calculations. E.A. Kanareykin and A.I. Kagramanyan: writing — original draft, calculations, and visualization.

Data Availability Statement

No data was used for the research described in the article.

References

[1] Tishin, A.M. and Spichkin, Y.I., 2003. The Magnetocaloric Effect and Its Applications. Bristol: Institute of Physics Publishing.

[2] Jahedmadieh, E. and Ehsani, M.H., 2026. Synthesis and Investigation of Structural and Magnetic Properties of Double Perovskite $PrBaMn_2O_6$. *Progress in Physics of Applied Materials*, 6(3), pp.257-263.

[3] Žužić, A., Barišić, D., Macan, J. and Pajić, D., 2025. Exploring the impact of synthesis method and dopant concentration on the magnetism and magnetocaloric effect of Sr-doped lanthanum manganites. *Journal of Applied Physics*, 137(14), 143901.

[4] Miri, A., Ehsani, M.H. and Esmaeili, S., 2023. Structural and electrical properties of gadolinium-substituted $La_{0.6-x}Gd_xSr_{0.4}MnO_3$ (x = 0–0.3). *European Physical Journal Plus*, 138, Article 1.

[5] Admi, R.I., Kurniawan, B., Saptari, S.A., Yudharma, G. and Munazat, D.R., 2024. Effect of sintering temperature on phase characteristic and grain size of $La_{0.7}AE_{0.3}MnO_3$ (AE=Ba/Ca/Sr) ceramics prepared by sol-gel method. *Progress in Physics of Applied Materials*, 3(1), pp.45-52.

[6] Raoufi, T. and Shokrian, F., 2021. Study of Landau theory and universal curve on $La_{0.6-x}Gd_xSr_{0.4}MnO_3$ (x = 0-0.1) manganite. *Progress in Physics of Applied Materials*, 1(1), pp.39-43.

[7] Gamzatov, A.G., Aliev, A.M., Abdulvagidov, S.B., Batdalov, A.B., Gorbenko, O.Y. and Kaul, A.R., 2007. Thermal and transport properties of manganites $Nd_{1-x}Sr_xMnO_3$ (x = 0.5, 0.45). *Physica B: Condensed Matter*, 395, pp.151–154.

[8] Fang, J., Li, X., Wang, Y., Luan, X. and Zhang, L., 2021. Nitrogen-doped $Ti_3C_2T_x$ MXene induced by plasma treatment with enhanced transport and structural properties. *Plasma Processes and Polymers (or related tracking)*, 18(11), p.2100120.
[9] Chen, L., Shi, X., Yu, N., Zhang, X., Du, X. and Lin, J., 2018. Measurement and analysis of thermal conductivity of $Ti_3C_2T_x$ MXene films. Materials, 11, Article 1701.
[10] Osborn, J.A., 1945. Demagnetizing factors of the general ellipsoid. *Physical Review*, 67, pp.351–357.
[11] Lienhard IV, J.H. and Lienhard V, J.H., 2020. A Heat Transfer Textbook. 5th edn. Cambridge, MA: Phlogiston Press.